JCTC Journal of Chemical Theory and Computation

ARTICLE

pubs.acs.org/JCTC

Solution Structure and Dynamics of Ni^{2+}(aq) from First Principles

Jiří Mareš,*,† Helmi Liimatainen,‡ Kari Laasonen,§ and Juha Vaara†

†NMR Research Group, Department of Physics, University of Oulu, P.O. Box 3000, FIN-90014, Oulu, Finland

‡Laboratory of Physical Chemistry, Department of Chemistry, University of Helsinki, P.O. Box 55 (A. I. Virtasen aukio 1), FIN-00014, Helsinki, Finland

§Laboratory of Physical Chemistry and Electrochemistry, Department of Chemistry and Materials Science, Aalto University, P.O. Box 16100, FIN-00076, Espoo, Finland

Supporting Information

ABSTRACT: The aqueous solution of Ni^{2+} was investigated using first principles molecular dynamics (FPMD) simulation based on periodic density-functional theory (DFT) calculations. The experimental structural parameters of the Ni(aq) complex are reproduced well by the simulation. An exchange event of the water molecule in the first solvation shell is observed, supporting the proposed dissociative mechanism of exchange. The calculated dynamic characteristics of the surrounding water molecules indicate too slow translational diffusion in comparison to experimental results, in agreement with other FPMD studies employing a similar level of theory. We also find that the reorientational dynamics of water are an order of magnitude slower as compared to experimental data. On the other hand, the angular momentum dynamics are in better agreement with the experimental data than the previously reported results from MD simulations employing empirical force fields. The obtained MD trajectory can supply accurate structures for the calculation of magnetic properties.

INTRODUCTION

The structure of hydrated multivalent ions is notoriously problematic to describe by classical nonpolarizable force fields. The case of the hydrated Ni^{2+} ion has been studied experimentally by neutron scattering and X-ray methods[1−3] and computationally using molecular dynamics (MD) simulations.[4−10] In the latter context, force fields have been developed that correctly model the average octahedral coordination of Ni^{2+} with six surrounding water molecules in the first solvation shell; however, the details differ among the various modeling studies. The problem originating from water polarization in the ion vicinity has been treated by an effective nonpolarizable two-body potential,[6,9] combined quantum mechanics/molecular mechanics (QM/MM) approach,[7,8,10] and, for a few different ions, accurately parametrized polarizable force fields.[11−13] As a further possible approach, first-principles molecular dynamics (FPMD) has been utilized for ion solvation.[14−20] It can be *a priori* assumed that FPMD should be superior to the other approaches, since it naturally includes polarization as well as other many-body effects. Within FPMD, one does not need to parametrize the ion−water potential and incorporate it into a particular water force field. The QM/MM approach lacks uniformity of description of the whole system, as manifested, e.g., in the practical difficulty in dealing with the exchange of molecules between the QM and MM regions. FPMD, on the other hand, treats the solvent−solvent as well as solvent−ion interactions on an equal footing. The FPMD steps require, however, either the diagonalization of the electronic Hamiltonian as well as subsequent force evaluation or an effective algorithm such as that due to Car and Parrinello[21] for approximately following the Born−Oppenheimer surface.[22] Consequently, FPMD is computationally expensive, limiting the length of the simulations as compared to parametrized empirical models. Furthermore, the underlying electronic structure method, usually density-functional theory (DFT), imposes its own restrictions on the accuracy of the intermolecular forces, as the van der Waals dispersion interaction is not well-described at standard DFT levels.[23] Properties of liquid water obtained from FPMD simulations have been discussed extensively.[24−30] Depending on the level of theory used in FPMD, primarily, the choice of the exchange-correlation functional (ECF), substantially varying structural (e.g., interatomic distances described by radial distribution functions, RDFs) and dynamical (e.g., translational and rotational diffusion) properties of water are obtained.

This work reports a very extensive FPMD simulation of the Ni^{2+} ion in aqueous solution. We investigate a variety of structural and dynamical properties. In the first part of this paper, we carefully investigate the RDFs between Ni^{2+} and the water atoms, the O−Ni−O angle distribution revealing the arrangement of ligand molecules around the Ni^{2+} ion, and the tilt angle of water molecules of the first and second solvation shells (FSS and SSS, respectively). Furthermore, we report the RDFs among the water atoms, their translational and rotational diffusion, and the angular momentum dynamics.

The six- as well as five-coordinated cases represent the prevailing situations in the solution as well as the fleeing intermediate occurring in the dissociative exchange reaction in the FSS, respectively. We were able to witness one such exchange process in our FPMD simulation, which is longer than comparable first-principles studies hitherto performed.

The paper is organized as follows: We start with a quantum-chemical (QC) study of the static structure of the unsolvated

Received: May 10, 2011
Published: July 27, 2011

hexa-aqua $Ni(H_2O)_6^{2+}$ complex, giving information on the performance of DFT ECFs against correlated *ab initio* calculations. Results from the static structure calculations are linked to the results from the FPMD simulation and compared to experimental data. Subsequently, the following sections are dedicated to the structure of the solution reported via RDFs, tilt angles, ligand−central ion−ligand angles, and dynamic properties such as self-diffusion coefficients, as well as reorientational and angular momentum correlation functions. Finally, details of the exchange process are reported.

METHODS

Quantum-Chemical Calculations. The FSS of the aqueous nickel ion, $Ni(H_2O)_n^{2+}$ (n = 5, 6), was investigated via structure optimization. For the structure optimization of the static FSS models, DFT in the ORCA program[31] was used with different ECFs (PBE, PBE0,[32,33] BLYP,[34−36] B3LYP,[35,37,38] BHandHLYP[39]). Spin-scaled second-order Møller−Plesset theory (SCS-MP2[40]) was used for comparison. Basis sets from the def2-XVP (X = S, TZ, aug-TZ, QZ) series[41] were used. The PBE functional was selected for the FPMD simulation.

First Principles Molecular Dynamics. The initial configurations of systems containing one Ni^{2+} and either 127 or 255 water molecules were prepared using empirical MD in the GROMACS 4 code.[42] The size of the cubic simulation box corresponds to experimental water density at 343 K with the side lengths of 19.8591 Å used for 255 water molecules and 15.7622 Å for 127 molecules. The boxes accommodate well both FSS and SSS; in particular, the latter has the shape of a sphere with a roughly 10 Å diameter. The two different system sizes were simulated to be able to test finite size effects on the static and dynamic characteristics important for the current and future calculations of molecular properties.

The production trajectories were run using Born−Oppenheimer MD with DFT forces calculated "on the fly", as implemented in the QUICKSTEP[43] module of the CP2K package.[44] In QUICKSTEP, a combination of the atom-centered Gaussian basis set and auxiliary plane waves (PW) is used. The PW basis is used together with the Gaussian basis to expand the electron density. The method employs a pseudopotential on each atom. For water, we tested DZVP, TZVP, TZV2P, and QZV3P valence basis sets.[43] The Ni−O distance in the $Ni(H_2O)_6^{2+}$ complex is well-converged already using the DZVP basis set, which was therefore selected for production runs. The Goedecker−Teter−Hutter pseudopotentials[45] for the PBE functional were used. For the Ni^{2+} ion, the DZV basis set available in CP2K in combination with a pseudopotential spanning 18 core electrons was used.

Furthermore, we investigated the dependence of the Ni−O distance in the $Ni(H_2O)_6^{2+}$ complex on the cutoff kinetic energy of the plane waves. Calculations using 1200, 600, 310, 280, and 250 Ry cutoffs for the larger simulation box revealed that 310 Ry yields a converged Ni−O distance. This cutoff was used for both sizes of the simulation box.

We tested the choice of the integration time-step of the equations of motion, which were propagated using the velocity Verlet algorithm.[46] Among the tested values 0.5, 0.7, 1, and 2 fs, the total energy of the Ni^{2+}/127 H_2O system within the *NVE* ensemble was well-conserved (drift 3.0×10^{-7} au/ps) using the 1 fs time-step, provided that a sufficiently tight self-consistent field (SCF) convergence criterion ($\varepsilon_{SCF} = 1 \times 10^{-7}$a.u.) was used.

The systems with 127 and 255 water molecules (both with one Ni^{2+} ion) were simulated for the total lengths of 90 and 33 ps of production trajectories, respectively. The simulation boxes, which were prepared using the classical force field in the GROMACS code, were further equilibrated in the initial phase of the FPMD simulation. The velocity scaling thermostat was used to prepare the system at the desired temperature of 343 K. Later, the production simulations continued in the *NVE* ensemble. The temperature was monitored, and the Ni−O radial distribution function (RDF) was monitored in the thermalization phase, until a stable situation was reached. The RDFs were calculated using VMD.[47] The self-diffusion coefficient D was calculated using the Einstein relation[48]

$$\langle |\mathbf{r}(\tau) - \mathbf{r}(0)|^2 \rangle = 6D\tau \quad (1)$$

where $\mathbf{r}(\tau)$ is the position of the center-of-mass of the water molecule at time τ, and the angular brackets denote averaging over molecules and time origins. Reorientational dynamics of the water molecules was investigated via the autocorrelation function of the principal axes of the moment of inertia tensor $\mathbf{I}$. For the principal axis $\hat{i}$, the relation for the unnormalized function at time offset τ is written as

$$C_{i_a}^n(\tau) = \langle P_n(\cos\theta_a) \rangle, a = x, y, z \quad (2)$$

$$\theta_a = \angle(\hat{i}_a(0), \hat{i}_a(\tau)) \quad (3)$$

where P_n is the nth order Legendre polynomial. The angular momentum correlation function was calculated in the Eckart frame[49,50] to minimize the vibrational contributions. The formula for the correlation function at time offset τ is written

$$C_{l_a}(\tau) = \langle l_a(0)\, l_a(\tau) \rangle, a = x, y, z \quad (4)$$

where l_a is the Cartesian angular momentum component along the a axis of the molecule-fixed Eckart frame.

RESULTS AND DISCUSSION

Structures of $Ni(H_2O)_6^{2+}$ and $Ni(H_2O)_5^{2+}$ Complexes. A schematic illustration of the hexa-aqua and penta-aqua complexes of Ni^{2+} is given in Figure 1. The basis-set requirements and the effect of the choice of ECF were first tested on the geometry parameters of the $Ni(H_2O)_6^{2+}$ complex, evaluated primarily via the Ni−O distance. The results are shown in Tables 1 and 2. The broad range of existing experimental data encompasses essentially all of our computational results. In the calculations using the ORCA code at the PBE level, the Ni−O distance of 2.086 Å was converged using the def2-TZVP basis set (*in vacuo*), which was then used for further tests of hexa-aqua Ni^{2+} structure. Periodic CP2K calculation of the finite $Ni(H_2O)_6^{2+}$ system using the same functional converges at a slightly longer distance, possibly due to the fact that pseudopotentials are used in CP2K. The r(Ni−O) distance and the tilt angle between the Ni−O vector and the bisector of the OH vectors of a water molecule behave systematically as functions of the exact exchange admixture in the ECF. The hybrid functionals lead to a shorter distance and smaller angle. In particular, *in vacuo*, the tilt angle using hybrid DFT or SCS-MP2 practically vanishes. With the COSMO solvation models, however, the results are brought into quantitative agreement with experimental results by the increase of the

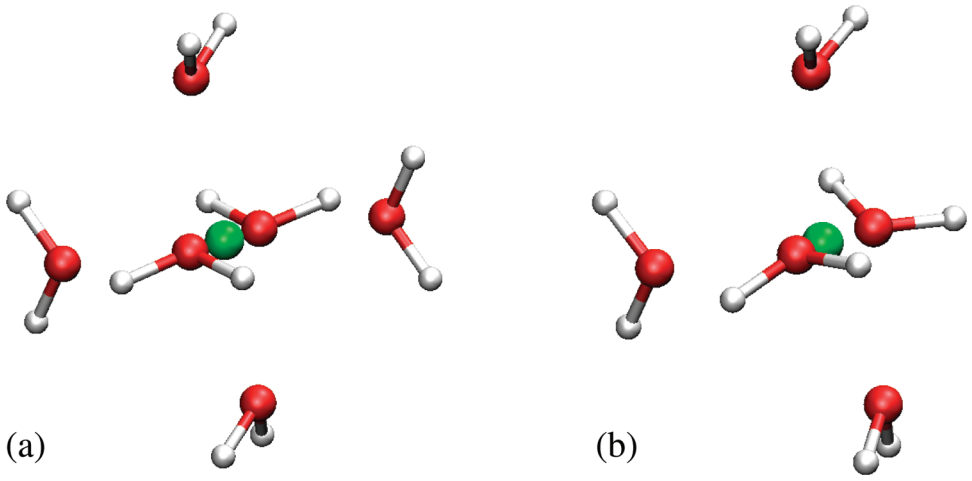

Figure 1. Structures of (a) $Ni(H_2O)_6^{2+}$ and (b) $Ni(H_2O)_5^{2+}$ obtained by geometry optimization at the SCS-MP2/def2-TZVP level using the COSMO solvation model. The positions of the water molecules are close to octahedral symmetry also in the penta-aqua complex.

Table 1. Basis-Set Dependence of the Distance (Å) between the Nickel Atom and Oxygen, r(Ni−O), in $Ni(H_2O)_6^{2+}$ [a]

program	r(Ni−O) with indicated basis sets				exptl.[b]
Orca	def2-SVP	def2-TZVP	def2-aug-TZVP	def2-QZVP	
	2.073	2.086	2.086	2.086	2.05−2.15
CP2K	DZVP	TZVP	TZV2P	QZV3P	
	2.100	2.089	2.093	2.092	

[a] The PBE functional was used in density-functional calculations *in vacuo*. For the CP2K calculation, the plane wave cutoff was set to 280 Ry in a cubic box with the side length 19.8591 Å. [b] See Table 3 for a more detailed list of values and references.

tilt angle to 33−46°. At the same time, a notable decrease of 1−2 pm in the r(Ni−O) distance takes place. Of the two tested GGA functionals (PBE and BLYP), PBE performs better for the structure as compared to the reference SCS-MP2 structure. The "optimal" amount of exact exchange appears to be somewhat below the 50% of BHandHLYP.

In general, due to error cancellation between the exact-exchange and pure DFT components, hybrid functionals lead to smaller self-interaction or, alternatively, delocalization error than pure GGAs.[51] Because of their additional computational cost, the hybrid functionals could not, however, be considered for the FPMD simulation of the required trajectory length and system size.

The structure of the 5-fold coordinated Ni^{2+} complex has also been calculated, as the $Ni(H_2O)_5^{2+}$ is the composition of the FSS of the transition structure during the exchange of coordinating water molecules. The structural parameters are listed in Table S1 (Supporting Information). Since the water molecules in $Ni(H_2O)_5^{2+}$ are not equivalent, we report values for each molecule separately. On average, however, the length r(Ni−O) is shorter compared to the 6-fold coordinated Ni^{2+} ion, whereas the average tilt angle does not differ significantly between the 5- and 6-fold structures.

Electronic Structure of $Ni(H_2O)_6^{2+}$ and $Ni(H_2O)_5^{2+}$ Complexes. In the companion article,[52] we thoroughly discuss the molecular magnetic properties obtained from the QM calculation. For the open-shell system, spin density is one such property quantitatively manifested in hyperfine coupling constants of the water nuclei. Here, we state only a few things. The discussion refers to single-point calculation on structures optimized by the corresponding method.

Comparing calculations with different DFT functionals, we see a systematic increase of the gap between the highest occupied and lowest unoccupied "α-spin" orbitals with an increasing amount of exact exchange. The same holds for the "β" orbitals. The finding is fully analogous to the commonly known trend of a HOMO−LUMO gap in closed-shell systems. The same is true for five- and six-fold coordinated complexes. In the case of the six-fold coordination, the two singly occupied molecular orbitals (SOMO) are almost exactly degenerate with energies differing by ca. 0.002−0.02 eV. The situation is different for the 5-fold coordinated complex for which the two SOMOs have an energy difference increased to the order of 0.1 eV, which in a qualitative way relates to the less symmetric structure of the five-coordinated complex.

Ni^{2+} Solvation Structure in Liquid Solution. In agreement with the accepted opinion, the Ni^{2+} complex is predominantly 6-fold coordinated in our FPMD trajectory. The main structural parameters of the hexa-aqua complex are summarized in Table 3, along with selected literature results. From the FPMD simulations, the maxima of the Ni−O and Ni−H RDF (*vide infra*) lie at 2.105 Å and 2.705 Å, respectively. The geometry optimization of $Ni(H_2O)_6^{2+}$ without dynamical corrections and using the COSMO solvation model at the PBE/def-TZVP level resulted in a Ni−O distance of 2.076 Å (Table 2). The ϕ(ONiO) angle values would in our case of octahedral geometry be expected at 90° and 180°. The ϕ(ONiO) angle of the six-coordinated ion, reported in Table 3, is very close to these values. The simulated distribution of the angle is given in Figure S1 of the Supporting Information. The 5-fold coordinated intermediate preserves to a large extent the octahedral symmetry. The same feature was observed during the optimization of the 5-fold coordinated ion (Figure 1). In the 5-fold part of the FPMD trajectory, the Ni−O and Ni−H distances are contracted by 6−7 pm as compared to the 6-fold case.

The tilt angle of water molecules around the central ion, reported in Table 3, is defined as the angle between the ion−oxygen vector and the bisector of the HOH angle. In contrast, θ is the angle between the ion−oxygen vector and the plane of the

Table 2. Dependence on the DFT Exchange-Correlation Functional of the Distance (Å) between the Nickel Atom and Oxygen, r(Ni−O), and the Tilt Angle [$\angle$(NiO,OH$_2$), (deg)] of Water Molecules in $Ni(H_2O)_6^{2+}$ [a]

solvation model	parameter	BLYP	B3LYP	BHandHLYP	PBE	PBE0	SCS-MP2	exptl.[b]
COSMO	r(Ni−O)	2.098	2.074	2.061	2.076	2.057	2.066	2.05−2.15
	$\angle$(NiO,OH$_2$)	44.1	37.7	30.7	45.7	38.4	33.0	0−50
in vacuo	r(Ni−O)	2.109	2.086	2.078	2.086	2.069	2.082	
	$\angle$(NiO,OH$_2$)	22.0	2.3	2.5	23.0	3.1	0.1	

[a] The tilt angle is illustrated in Figure S2 of the Supporting Information. Both calculations were performed with the Orca program, *in vacuo* or using the COSMO solvation model as indicated. The def2-TZVP basis set was used. For comparison, SCS-MP2 and experimental results are also given. [b] See Table 3 for a more detailed list of values and references.

Table 3. Structural Characteristics of the Aqueous Solution of Ni^{2+} [a]

	r(Ni−O) (Å)	r(Ni−H) (Å)	$\angle$(NiO,OH$_2$) (deg)	ϕ(ONiO) (deg)
FPMD(6)[b]	2.11	2.71	43.5	89−90, 172−173
FPMD(5)[c]	2.05	2.64	44.0	89−90
QM/MM[d]	2.14	2.81	∼0	89.1, 172.7
MD	2.06,[e] 2.06[e]	2.67,[f] 2.76[f]	∼35,[e] ∼0[f]	∼90[f]
exptl.	2.05−2.10(2.15),[g,h] 2.072,[i] 2.05[j]	2.77[i]	30, 40,[g,k] 0−42,[l] 42,[m] ∼0[i]	∼90, 180[i]

[a] The location (Å) of the first maxima of Ni−O and Ni−H radial distribution functions, the tilt angle of water molecules $\angle$(NiO,OH$_2$) (deg,) and the oxygen−nickel−oxygen average angle ϕ(ONiO) (deg) in the first solvation shell of Ni^{2+} are listed. [b] This work, first principles molecular dynamics using the PBE functional and the model with 128 water molecules. The part of the trajectory with a 6-fold coordinated Ni^{2+} ion. [c] As footnote *b*, but for the part of the trajectory with a 5-fold coordinated Ni^{2+} ion. [d] Ref 8. Quantum mechanics/molecular mechanics with the UHF/double-ζ/Los Alamos effective core potential (Ni) level of theory used for QM. [e] Ref 6. Empirical MD using a nonpolarizable force field. [f] Refs 3 and 9. Empirical MD using a nonpolarizable force field. [g] Reviewed in ref 1, with original literature cited therein. [h] Range of 26 experimental results from X-ray diffraction, EXAFS, and neutron diffraction. Only one report of 2.15 Å. [i] Ref 3. Extended X-ray absorption fine structure (EXAFS). [j] Ref 2. EXAFS. [k] Neutron scattering data. [l] Ref 53. Neutron scattering, 0 ± 20° at low concentration, 34 ± 8 or 42 ± 8° at 4.4 M. [m] Ref 54. Neutron scattering.

water molecule, which is defined by its normal vector. Figure S2 (Supporting Information) illustrates the two definitions as well as the simulated distributions of the two angles. In the FSS, only a small difference between θ and tilt angle exists, so they are not distinguished in further discussion. A broad range of tilt angles have been reported for the aqueous Ni^{2+} solution. Numerous older experimental data[1,53,54] show a tilted geometry, while a newer EXAFS study[3] is in agreement with angle oscillating around 0°. Inada et al.[8] reported, using the QM/MM method, a flat maximum around 0°, using the modest unrestricted Hartree−Fock level of theory for the QM part. Chillemi et al.[9] developed an empirical potential according to the experimental results of D'Angelo et al.[3] Classical MD using this potential also resulted in an around-zero tilt angle. Odelius et al.[6] obtained the angle of 35° from a classical MD simulation in a study concerning magnetic properties.

In agreement with the majority of experimental data, the current FPMD trajectories show an average tilt angle significantly distinct from zero. The average value from the 6-fold coordinated part of the FPMD trajectory is 43.5°, and the maximum of the distribution is near 47°. The same angle was observed in our simulations with both 127 and 255 solvent molecules. Static $Ni(H_2O)_6^{2+}$ structures (Table 2) obtained by optimization in implicit (COSMO) water also yielded a tilted water geometry (angle of ca. 45° at PBE level), representing very well the FPMD distribution. Hybrid functionals yield a somewhat less tilted geometry at 30−38°, however.

FPMD simulations of solvated paramagnetic ions have seldom been reported. Hence, there are very few data at the first principles level with which the present findings can be compared. As an example, in a simulation of the gadolinium ion reported by Yazyev and Helm,[55] an average tilt angle of 35° was obtained, whereas the experimental values in that case range between 10° and 24°.[1] In contrast, distribution of the tilt angle was found to be rather narrow, centered around zero degrees when using classical MD together with a polarizable force field.[11] It remains somewhat unclear how well the tilt angle distributions obtained presently for Ni^{2+} reflect the physical reality since the range of experimental results is very broad.

The distributions of the tilt and θ angles in SSS are also depicted in Figure S2 (Supporting Information). The two differently defined angles have differing distributions in SSS, in contrast to FSS. Both distributions are much broader than in FSS, reflecting the much stronger orientational bias in FSS. The SSS tilt angle distribution has two flat maxima, one around 50° where the oxygen is directed toward the central ion, reminiscent of the prevailing situation in FSS. The second maximum corresponds to the oxygen atoms pointing outward (the ∼105° local maximum in Figure S2). Distribution of the θ angle shows that there is vanishing probability for the plane of the water molecule to be perpendicular to the oxygen−ion vector.

Structure of the Surrounding Water. The parameters of the simulated RDF of the water atoms as well as published data (the latter obtained for pure water) are summarized in Table 4. It is known from the literature and also apparent from Table 4 that FPMD based on DFT tends to overstructure water. This is shown both in the O−O and H−H RDF peak locations that are found at values that are slightly smaller than in the experimental data and in the heights of the peaks that are too large. Whereas the height of the first experimental maximum of the O−O RDF falls into the range of 2.6−2.8, FPMD based on PBE typically predicts values over 3.2. Our work is well in line with the FPMD studies of pure water using the PBE functional,[26,29,28] implying a very small relative effect of the ion on the average water structure

Table 4. Comparison of the Position of the Simulated Maxima (r_{max}) and Peak Values (g_{max}) of Intermolecular Radial Distribution Functions of Liquid Water from the First Principles Molecular Dynamics Simulation of the Aqueous Solution of the Ni^{2+} Ion (This Work) and Pure Water (Literature)[a]

method	r_{max}^{OO} (Å)	g_{max}^{OO}	r_{max}^{OH} (Å)	g_{max}^{OH}	r_{max}^{HH} (Å)	g_{max}^{HH}
FPMD/PBE[b]	2.71/4.4	3.25/1.42	1.71/3.22	1.70/1.63	2.25/3.80	1.76/1.23
MD[c]	2.82/4.62	3.15/1.11	1.86/3.30	1.52/1.62	2.44/3.82	1.56/1.17
FPMD/BLYP[d]	2.82−2.84	3.12−3.24				
FPMD/BLYP-D[d]	2.80	2.78				
FPMD/PBE-D[d]	2.76	3.35				
FPMD/PBE	2.76,[d] 2.73,[e] 2.70[f]	3.28−3.54,[d] 3.25,[e] 2.99[f]				
FPMD/PBE0	2.74[f]	2.58[f]				
exptl.[g]	2.76/4.52	2.62/1.15	1.78/3.31	1.11/1.52	2.35/3.85	1.28/1.17
	2.8/4.5[h]	2.8/1.13[h]				

[a] The columns contain the properties of the first/second maximum if both are available. [b] This work; parameters extracted from the analysis of all water molecules regardless of their localization in the solvation structure of the ion. The values are identical for the smaller (127 water molecules) and larger (255) simulated systems. [c] Empirical MD using the polarizable AMOEBA force field.[56] [d] Ref 28. "D" in BLYP-D and PBE-D indicates the dispersion correction.[57,58] [e] Ref 29. [f] Ref 26. [g] Ref 59. Neutron diffraction. [h] Ref 60. X-ray scattering.

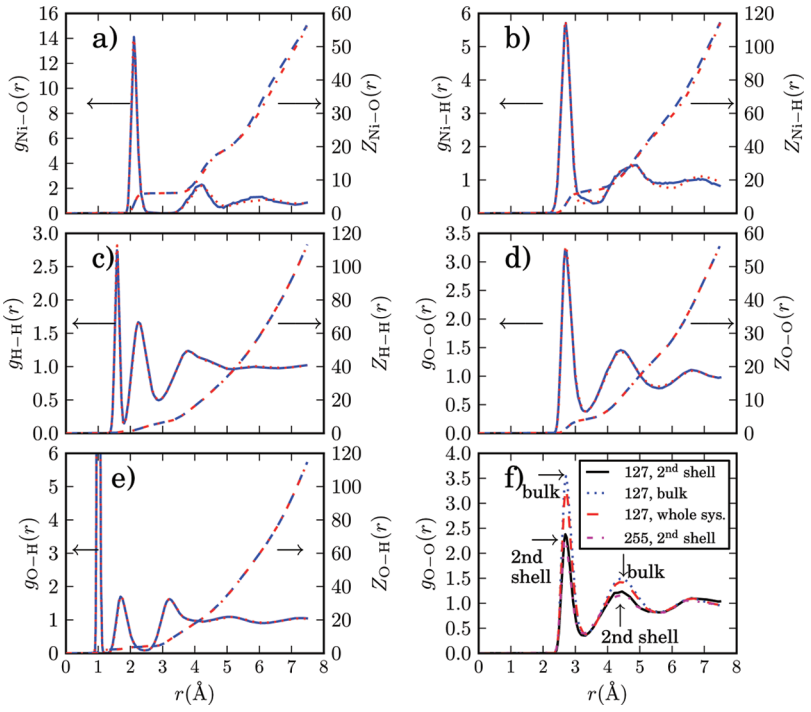

Figure 2. Radial distribution functions $g(r)$ and running coordination numbers $Z(r)$ in the first principles molecular dynamics simulations of the aqueous solution of the Ni^{2+} ion. (a) Ni−O, (b) Ni−H, (c) H−H, (d) O−O, (e) O−H, and (f) O−O RDFs. The solid blue and dotted red lines represent the RDF curves for the simulation containing 255 (33.75 ps) and 127 (90 ps) water molecules, respectively. The dashed blue (255) and dash-dotted red (127) lines represent the running coordination numbers. Panel f shows the differences in the radial distribution functions between the bulk water and the water molecules of the second coordination shell.

in our simulation. In the work of Schmidt et al.,[28] an empirical dispersion correction[57,58] is included. The best results are obtained using BLYP-D, which in a constant pressure simulation also results in a nearly experimental water density. The role of the "D" correction on the static structure may, however, be relatively small, as the PBE calculations with and without the dispersion corrections produce practically similar results. It appears that the computationally demanding hybrid DFT functionals also lead to some improvements over FPMD performed using GGA functionals.[26] The structural properties of water obtained from the classical AMOEBA[56] model, which is generally considered good for the water structure and dynamics, produces overestimated interatomic distances, in contrast to the underestimation found for FPMD. However, the RDF peak values remain too large with the empirical simulation.

The features of the intrawater O−O, O−H, and H−H RDF curves in Figure 2 are practically identical for both simulations, with 127 and 255 water molecules. In contrast, the Ni−O and Ni−H RDFs show small differences between the two simulations after the first maximum. The O−O RDF calculated separately for SSS is shifted by ca. 0.02 Å toward a shorter distance, indicating the effect of the central ion (Figure 2f). The height of the

maximum of the second shell RDF is lowered as compared to the bulk simulation by the fact that the molecules in the SSS have on average fewer neighbors than the molecules of the bulk.

We have neglected the effects of the quantum dynamics of the nuclei. Specialized simulations with path-integral treatment of quantum effects[61,62] are reported to perform better than the classical dynamics models, giving RDFs very close to the experimental results for liquid water.

Translational Diffusion in Water. In contrast to the average structural properties of water, the dynamic properties obtained by the different methods span a much broader range. Literature reports about dynamic properties of water by FPMD are by and large restricted to the coefficient of translational diffusion D. Therein, FPMD delivers results that deviate by an order of magnitude from the experimental values.[25−30] From Table 5, we can observe that the diffusion coefficients D that we obtain for water in the aqueous solution of Ni^{2+} are near the GGA-based FPMD simulations of pure water by others but are clearly too small as compared to the experimental results. D resulting from the larger simulation box is doubled with respect to the results corresponding to the smaller box. This may indicate a finite size effect due to insufficient size of the simulation cell. Indeed, the results of the corresponding FPMD simulation of pure water[29] give a still larger value, when extrapolated to an infinite box size. We have to point out, however, that the average simulation temperature of the bigger system was almost 10 K higher in our work, which influences the numerical values. It is noteworthy that hybrid DFT-based FPMD led to much improved diffusion constants,[26] in qualitative agreement with the experiment. A high-quality empirical simulation using a polarizable force field (but also other force fields not listed here) also provides better data than obtained with FPMD using the PBE functional.

Rotational Dynamics in Water. The reorientational correlation times are compared in Table 5. To be able to relate our results to the available experimental data, we calculated the rotational correlation functions associated with both the first- and second-order Legendre polynomials, eq 2. To obtain the correlation time τ, we calculated the integrals of the normalized correlation function:

$$\tau = \int_0^\infty c(t)\,\mathrm{d}t \tag{5}$$

$$c(t) = \frac{C(t)}{\langle C(0)\rangle} \tag{6}$$

in which the dominant first part was obtained by numerical integration, whereas the tail region was integrated analytically after extrapolation by a fitted biexponential function. We also report τ obtained via an alternative route, corresponding directly to a biexponential fit to the correlation function. Since the two fit parameters are sensitive to the sampling of the trajectory, we only report the longer τ corresponding to the tail region. The shorter time, corresponding to the fast-decaying exponent, reflects the initial, complex behavior of the correlation function.

Ultrafast time-resolved experimental data[66] imply that the reorientational dynamics differ from simple diffusive rotation. A jump model of water reorientation was recently described, e.g., in refs 63, 68−70. The details of the reorientational dynamics are essential, for example, for the correct evaluation of the NMR relaxation data, see, e.g., ref 71. There are, however, no other FPMD studies available for comparison with our simulation. The

Table 5. Comparison of the Self-Diffusion Coefficient D As Well As τ_1 and τ_2 Correlation Times of the Rotational Autocorrelation Functions for Pure Water (Literature Values) and an Aqueous Solution of Ni^{2+} (Present Work)

method	D (Å^2/ps)	τ_1 (ps)[a]	τ_2 (ps)[a]	temperature (K)
FPMD/PBE[b,c]	0.02	38, 34	26, 18	368
FPMD/PBE[c,d]	0.04	33, 30	21, 16	378
FPMD/PBE[e]	0.047			350
FPMD/PBE0[e]	0.28			350
FPMD/PBE[f]	0.079			300
MD	0.202[g,h]	6.6[g,i]	3.5[g,i]	298
exptl.	0.23[j]		2.5[k]	298
exptl.[l]		0.7,13		
exptl.[m]			2.07	313

[a] The correlation times τ_1 and τ_2 are simulated using first- and second-order Legendre polynomials, eq 2. [b] This work; first-principles molecular dynamics using the PBE functional, 127 water molecules. [c] Two values for both the first- and second-order correlation times τ are presented: the longer time of a biexponential fit and the "integral" time, in this order (see text). [d] As footnote *b*, but for 255 water molecules. [e] Ref 26. To be compared with ca. 0.5 Å^2/ps of 350 K for D_2O. [f] Ref 29. Result extrapolated to an infinite simulation box size. [g] Ref 56. Empirical molecular dynamics using the polarizable AMOEBA force field. [h] Ref 56. [i] Ref 63. [j] Ref 64. Diaphragm-cell technique. [k] Ref 65. Femtosecond infrared pump−probe experiment. [l] Ref 66. Femtosecond infrared pump−probe experiment, two constants of biexponential decay, temperature not reported. [m] Ref 67. ^{1}H NMR relaxation.

numbers obtained from our work are three or more times larger than the experimental values. This implies a connection to the glassy behavior of FPMD water discussed, e.g., in refs 27, 72, and 73. Slow dynamics by FPMD are therefore manifested not only in the translational diffusion as described above but also in the reorientational dynamics. Comparison of the reorientational dynamics around the different molecule-fixed axes in Figure 3 indicates relatively similar dynamics in the FSS around the direction of the molecular dipole moment as well as that of the normal of the plane of the molecule. In contrast, hindered rotation around the remaining in-plane direction is observed. Beyond FSS, a somewhat faster, isotropic reorientational motion is seen.

Angular Momentum Dynamics in Water. Further insight into the dynamical properties of water is brought by the angular velocity correlation function or, when including the moment of inertia, the angular momentum correlation function. The results from our simulations are given in Table 6. Figure 4 compares the functions for the different molecular axes and different location in solution (FSS, SSS, and bulk). See Figures S3 and S4 (Supporting Information) for an analysis of the differences between the molecule-fixed axes and effects of the simulation cell size, respectively. The literature data in Table 6 include the available empirical MD simulations[74−76] and inelastic neutron scattering data.[77] Numbers from our simulation are those for the angular momentum correlation function that are, however, identical to those of the angular velocity correlation function within the reported precision. [For test purposes, both angular momentum and an angular velocity correlation function have been calculated and compared.] Clearly, the FPMD simulation produces, albeit at higher temperatures than in the other data, the time of first minimum closest to the experimental data. Among the empirical simulations, there are large differences in τ_{min} for

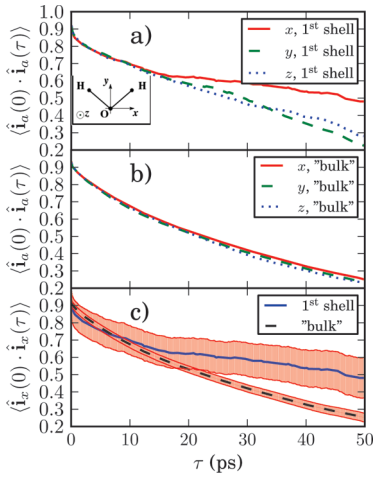

Figure 3. Reorientational correlation functions of the water molecule in aqueous Ni^{2+} from first-principles molecular dynamics simulation with 127 solvent molecules. The functions appropriate for the different molecule-fixed axes are illustrated in (a) first solvation shell and (b) bulk water as well as (c) the x direction in both. The inset of panel a indicates the choice of the molecule-fixed axis system. $\hat{\mathbf{e}}_a$ (a = x,y,z) denotes a unit vector along the molecular axis a. Panel c shows the uncertainty intervals for $a = x$ for the correlation functions of the first shell and bulk water. Here, "bulk" denotes all water molecules except those contained in the first solvation shell.

the two simulations at nearly identical temperatures using the MCYL and TIP4P force fields.[74,75] Differences between, on the one hand, the classical TIP4P model and, on the other hand, TIP4P with nuclear quantum effects appear to be of minor importance around room temperature. All of the simulations point to a slightly anisotropic behavior of the angular momentum correlation function, with the decay of the off-plane direction slightly slower than that in the two in-plane directions.

From the value of the angular momentum correlation function at its first minimum, we can reconfirm the previous observation that the intermolecular interactions within the FPMD simulation restrict the motion more than required. Nevertheless, the decay rate of the angular momentum is reproduced better than by classical force fields.

We further present a detailed analysis of the angular momentum correlation functions from our simulation in Figure 4 as well as in Figures S3 and S4 (Supporting Information). From Figure 4, it may be concluded that FSS, which interacts strongly with the metal ion, features faster fluctuations of the angular momentum than SSS and bulk water. The breakdown of the angular momentum correlation function in terms of the Cartesian components of $\mathbf{l}$ in molecule-fixed frame (Figure S3) reveals that the short time-scale dynamics are roughly isotropic, meaning that the angular momenta about the three molecular axes behave similarly. The two in-plane components l_x and l_y also behave similarly in SSS and bulk water, whereas the perpendicular component l_z exhibits the slowest time-scale.

There exists in FSS a regularly oscillating, slowly decaying angular momentum autocorrelation function, particularly in the y direction (molecular dipole moment) as compared to the more distant molecules from the ion. In Figure S4 (Supporting Information), the comparison of the smaller (127 water molecules) and larger (255) simulated systems is plotted for FSS and bulk water, here, molecules beyond FSS. From Figure S4

Table 6. Features of the Angular Velocity Correlation Function of Water Molecules in Simulated Aqueous Solution of Ni^{2+} Ion (This Work) or Pure Liquid Water (Literature)[a]

method	τ_{min} (fs)[b]	TCF_{min}[c]	temperature (K)
FPMD[d]	20, 20, 25	−0.68, −0.67, −0.68	368
MD[e]	45, 45, 55	−0.52, −0.54, −0.52	300
MD[f]	25, 29, 31	−0.59, −0.51, −0.58	298
MD[g]	25, 30, 32	−0.59, −0.48, −0.54	298
MD[h]	24, 24, 31	−0.5, −0.5, −0.5	286
exptl.[i]	14	−0.44	300

[a] Molecular axes are depicted in Figure 3a. [b] Literature numbers were extracted from published graphs. τ_{min} is the time of the first minimum corresponding to x, y, and z axes, in this order. [c] The value of the correlation function at the first minimum. [d] This work, first-principles molecular dynamics simulation of Ni^{2+} in liquid water (127 molecules, PBE functional). [e] Ref 74. *Ab-initio*-based parametrized empirical potential MCYL. [f] Ref 75. Empirical TIP4P simulation. [g] Ref 75. TIP4P with nuclear quantum effects. [h] Ref 76. MCY potential. [i] Ref 77. Inelastic neutron scattering.

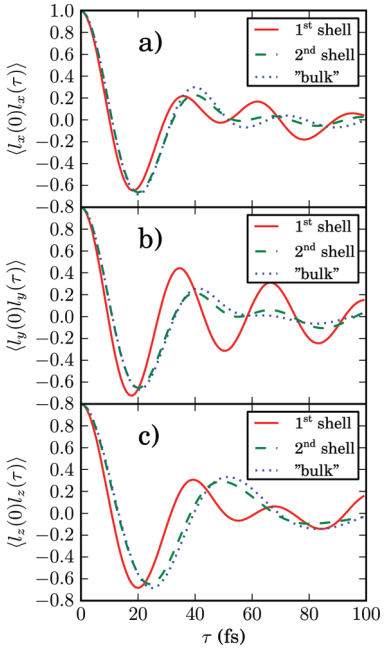

Figure 4. Angular momentum correlation functions of the water molecules in the aqueous solution of Ni^{2+} from first-principles molecular dynamics simulation with 127 water molecules. Comparison of the water property in the first and second solvation shells as well as bulk, for the different molecular axes. Here, "bulk" denotes all water molecules except those in the first and second solvation shells. See Figure 3a for the definition of the molecule-fixed axes.

(a−c), we observe that in the larger simulation box the periodic oscillations become significantly more damped for the FSS water molecules. There also exists a tiny difference in the rate of the oscillation: the smaller simulation box corresponds to slightly faster oscillations of $\mathbf{l}$. Since this observation applies only to FSS (the bulk water is practically unaffected), the difference cannot be explained by the 10 K difference in the simulation temperature of the smaller and larger system. The finite size of the periodic box clearly exaggerates the oscillatory behavior. Hence, one should be careful in FPMD simulations that require small simulation cells,

when evaluating data that depend on the angular momentum correlation functions or related dynamical properties of FSS. Figure S5 (Supporting Information) indicates that only a small difference exists between the angular momentum autocorrelation function $\langle \mathbf{I}(0)\cdot\mathbf{I}(\tau)\rangle$ for the $\mathbf{I}$ vector as calculated in the laboratory frame and the Eckart frame, the latter enabling the above-discussed breakdown into the different molecular-fixed axes $\langle \mathbf{I}_x(0)\cdot\mathbf{I}_x(\tau)\rangle$ etc.

As an overall conclusion, the present FPMD simulations result in structural parameters, in good agreement with the current knowledge. There are better results obtained for individual properties of pure water reported in literature. In our case, selecting the PBE functional resulted in balanced properties of the more complex system featuring ion solvation. The obtained trajectory should therefore be well-suited, e.g., for the calculation of average magnetic properties.[52] As hinted by the known issues regarding the translational diffusion constant by FPMD, the reorientational dynamics are also too slow in FPMD with PBE. In contrast, FPMD for angular momentum dynamics performs significantly better. FPMD calculations of dynamical properties require particular care.

The dispersion correction[57,58] was shown to improve properties of pure water calculated by the PBE functional, though even then the problem of overstructured water is only alleviated.[28] The dynamical properties should therefore also be shifted in the required direction. In the case of the PBE functional, an improvement in gas-phase energies has been seen in more complex systems of hydrated aluminum complexes, their hydrolysis proceeding a little faster and further compared to the uncorrected PBE functional.[20] To see how the interaction between water and Ni^{2+} is affected by the *a posteriori* dispersion corrections, we ran a simple potential energy scan of the Ni^{2+} ion and one water molecule with fixed geometry. The curves are nearly identical, as the dispersion correction is very small compared to the main electrostatic forces (data not shown). The influence of the empirical dispersion corrections on dynamical properties is an interesting topic for further investigation.

Exchange in the First Solvation Shell of the Ni^{2+} Ion. The mechanisms of the exchange of water molecules in the FSS of the Ni^{2+} ion have been discussed in the literature. A MD study by Inada et al.[8] using the Ni−O force field obtained at the unrestricted Hartree−Fock level, including a three-body correction, pointed to a dissociative mechanism. This means for the Ni^{2+} complex that the exchange proceeds via a 5-fold coordinated intermediate, i.e., one molecule leaves FSS before the new molecule arrives. However, the same authors concluded in a QM/MM study[7] that mainly the associative mechanism prevails. Later on, Loffler et al.[10] applied the umbrella sampling method[79] in a classical MD simulation using the same three-body-corrected potential as in ref 8 and reconfirmed the dissociative mechanism.

During our simulation with 127 water molecules, a water exchange event in FSS was observed to proceed via a 5-fold, long-lived intermediate. At the beginning of the process, the leaving water molecule gradually increases its Ni−O distance after being expelled by collisions with the other molecules in FSS. The increase of Ni−O distance from 2.15 to 3.75 Å takes 164 fs. After 4.8 ps, another molecule approaches the 5-fold coordinated complex. The shortening of the Ni−O distance (3.75 to 2.15 Å) takes 373 fs (Figure S6, Supporting Information). The five remaining water molecules largely retain the structure of the usual 6-fold coordination, similarly to the case of static quantum-chemical structures (Figure 1). Static calculations (not shown), in which one of the water molecules was pulled away by extending the Ni−O distance (with the structure otherwise relaxed), showed that the departing water molecule started to prefer hydrogen bonding with the remaining FSS water molecules over coordination with the ion, after $r_{Ni-O} \approx 3.1$ Å.

Observation of such a FSS exchange process for a divalent ion is uncommon in FPMD simulations, and unlikely even in our simulation where the trajectory was exceptionally long (taking into account the system size). To our knowledge, a corresponding observation has not been described in the literature. The dissociative mechanism that we observe is also in accordance with a high-pressure ^{17}O NMR experiment,[80] although by observing this single exchange event, no real conclusions can be made.

A simple calculation addressing the activation energy of the water-exchange mechanism has been done using the COSMO implicit solvation model. We calculated a relaxed surface scan of one water molecule leaving the 6-fold coordinated complex at the PBE/dev2-TZVP level (Figure S7, Supporting Information). We obtained a small potential well of 1.65×10^{-2} eV as compared with $k_BT \doteq 2.58 \times 10^{-2}$ eV at 300 K. At the same level of theory, the 7-fold coordinated structure is unstable, pointing also to the dissociative mechanism of water exchange, although this simple calculation completely neglects all the effects of dynamics and other effects of explicit solvation.

CONCLUSIONS

We have investigated using first-principles computations the structure and dynamics of the aqueous solution of Ni^{2+}. Both static quantum-chemical calculations of the hexa- and penta-aqua complexes $Ni(H_2O)_n^{2+}$ (n = 5, 6), as well as first-principles molecular dynamics simulation of the aqueous solution, were performed. The investigated properties were the radial correlation functions, translational diffusion constants, and reorientational and angular momentum correlation functions. The first principles trajectory is the longest of its kind so far, for system and properties of the present type. Two different simulation cells were used with 127 and 255 water molecules and one Ni^{2+} ion.

The detailed structure of the first solvation shell including six water molecules has been found sensitive to the computational level. The optimized r_{Ni-O} distance agrees well with the experiment both in the static hexa-aqua complex and in the radial distribution functions of the simulated trajectory. The most ambiguous structural feature of the hexa-aqua Ni^{2+} complex, and also very important for subsequent calculation of the magnetic properties of the solution, is the tilt angle of the water molecules. We show that the structure of the hexa-aqua Ni^{2+} complex calculated with an implicit solvation model has a tilt angle (∼45°) close to peak of the distribution in the first-principles MD (∼47°), when the same PBE exchange-correlation functional is used. The tilt angle is larger than experimental values (ranging between 30 and 42°), and it is likely that the actual equilibrium tilt angle is close to 33° obtained for the hexa-aqua complex by the reference SCS-MP2 method.

The extensive FPMD trajectory allowed us to study the dynamics of the aqueous Ni^{2+} complex including the dynamic properties of the surrounding water. Fortuitously, an exchange event of a water molecule in the first solvation shell occurred during the simulation, and we are, for the first time, able to support by first-principles calculation the suggestion that it proceeds by a dissociative mechanism through a 5-fold

coordinated intermediate, which to a significant extent preserves the octahedral symmetry.

The computed translational diffusion constant of the water molecules has been compared to the experimental and various computational results. The diffusion constant is lower by an order of magnitude than the experimental results in pure water. This is a common finding for the combination of FPMD and the PBE exchange-correlation functional. The calculated diffusion constants feature a pronounced dependence on the simulation cell size, with the larger system leading to somewhat improved agreement with experimental results. However, qualitatively correct results have only been obtained in the literature with either expensive hybrid DFT-based FPMD or by a number of modern, empirical force fields.

We fill a gap in the literature by evaluation of the rotational dynamics of the water molecules by FPMD. The obtained τ_1 correlation time is several times longer than published experimental results. τ_2, which is obtained from experiments much more frequently, differs from our simulation by roughly an order of magnitude. The slow dynamics implies that the properties that depend on either translational or rotational diffusion must be evaluated with special care in FPMD simulations. For example, the empirical AMOEBA simulations outperform the present FPMD simulation in this respect.

Angular velocity or angular momentum correlation time of liquid water are very seldom reported in the literature. This quantity is of relevance for the spin-rotation mechanism of NMR relaxation. Comparison with results from inelastic neutron scattering indicates good performance of FPMD for this property, yielding better results than empirical force fields. Evaluation of the correlation time for the first solvation shell of the Ni^{2+} ion in the smaller and larger simulation box reveals artifacts from periodic boundary conditions, when a small cell is used. The angular momentum dynamics of the first solvation shell are overall faster than in the second shell or bulk water.

■ ASSOCIATED CONTENT

Supporting Information. Additional figures related to the structural and dynamical properties of $Ni^{2+}(aq)$ as well as a table of functional dependence of the distances between the nickel atom and oxygen in $Ni(H_2O)_5^{2+}$. This material is available free of charge via the Internet at http://pubs.acs.org

■ AUTHOR INFORMATION

Corresponding Author
*E-mail: jiri.mares@oulu.fi.

■ ACKNOWLEDGMENT

The authors thank Dr. Perttu Lantto and Dr. Matti Hanni (Oulu) for helpful discussions. The research leading to these results has received funding from the European Union Seventh Framework Programme (FP7/2007-2013) under grant agreement no. 254552 (J.M.). Further support was received from Swiss National Funds - project PBZHP2-125353 (J.M.), University of Helsinki Research Funds, and the University of Oulu. J.M., H.L., and J.V. belong to the Finnish Center of Excellence in Computational Molecular Science (CMS). Computational resources due to CSC (Espoo, Finland) were used.

■ REFERENCES

(1) Ohtaki, H.; Radnai, T. *Chem. Rev.* **1993**, *93*, 1157.
(2) Inada, Y.; Hayashi, H.; Sugimoto, K.; Funahashi, S. *J. Phys. Chem. A* **1999**, *103*, 1401.
(3) D'Angelo, P.; Barone, V.; Chillemi, G.; Sanna, N.; Meyer-Klaucke, W.; Pavel, N. V. *J. Am. Chem. Soc.* **2002**, *124*, 1958.
(4) Bounds, D. G. *Mol. Phys.* **1985**, *54*, 1335.
(5) Natália, M.; Cordeiro, D. S.; Ignaczak, A.; Gomes, J. A. N. F. *Chem. Phys.* **1993**, *176*, 97.
(6) Odelius, M.; Ribbing, C.; Kowalewski, J. *J. Chem. Phys.* **1995**, *103*, 1800.
(7) Inada, Y.; Loeffler, H. H.; Rode, B. M. *Chem. Phys. Lett.* **2002**, *358*, 449.
(8) Inada, Y.; Mohammed, A. M.; Loeffler, H. H.; Rode, B. M. *J. Phys. Chem. A* **2002**, *106*, 6783.
(9) Chillemi, G.; D'Angelo, P.; Pavel, N. V.; Sanna, N.; Barone, V. *J. Am. Chem. Soc.* **2002**, *124*, 1968.
(10) Loffler, H. H.; Mohammed, A. M.; Inada, Y.; Funahashi, S. *J. Comput. Chem.* **2006**, *27*, 1944.
(11) Clavaguéra, C.; Calvo, F.; Dognon, J. P. *J. Chem. Phys.* **2006**, *124*, 74505.
(12) Piquemal, J.; Perera, L.; Cisneros, G. A.; Ren, P.; Pedersen, L. G.; Darden, T. A. *J. Chem. Phys.* **2006**, *125*, 54511.
(13) Villa, A.; Hess, B.; Saint-Martin, H. *J. Phys. Chem. B* **2009**, *113*, 7270.
(14) Lyubartsev, A. P.; Laasonen, K.; Laaksonen, A. *J. Chem. Phys.* **2001**, *114*, 3120.
(15) Bakó, I.; Hutter, J.; Pálinkás, G. *J. Chem. Phys.* **2002**, *117*, 9838.
(16) Lightstone, F. C.; Schwegler, E.; Allesch, M.; Gygi, F.; Galli, G. *ChemPhysChem* **2005**, *6*, 1745.
(17) Ikeda, T.; Boero, M.; Terakura, K. *J. Chem. Phys.* **2007**, *126*, 34501.
(18) Todorova, T.; Hünenberger, P. H.; Hutter, J. *J. Chem. Theory Comput.* **2008**, *4*, 779.
(19) Petit, L.; Vuilleumier, R.; Maldivi, P.; Adamo, C. *J. Chem. Theory Comput.* **2008**, *4*, 1040.
(20) Saukkoriipi, J.; Laasonen, K. *J. Chem. Theory Comput.* **2010**, *6*, 993.
(21) Car, R.; Parrinello, M. *Phys. Rev. Lett.* **1985**, *55*, 2471.
(22) Marx, D.; Hutter, J. *Modern Methods and Algorithms of Quantum Chemistry*, 2nd ed.; John von Neumann Institute for Computing: Jülich, Germany, 2000; Vol. 3, p 329.
(23) Hobza, P.; Šponer, J.; Reschel, T. *J. Comput. Chem.* **1995**, *16*, 1315.
(24) Laasonen, K.; Sprik, M.; Parrinello, M.; Car, R. *J. Chem. Phys.* **1993**, *99*, 9080.
(25) Kuo, I. W.; Mundy, C. J.; McGrath, M. J.; Siepmann, J. I.; VandeVondele, J.; Sprik, M.; Hutter, J.; Chen, B.; Klein, M. L.; Mohamed, F.; Krack, M.; Parrinello, M. *J. Phys. Chem. B* **2004**, *108*, 12990.
(26) Todorova, T.; Seitsonen, A. P.; Hutter, J.; Kuo, I. W.; Mundy, C. J. *J. Phys. Chem. B* **2006**, *110*, 3685.
(27) Lee, H.; Tuckerman, M. E. *J. Chem. Phys.* **2007**, *126*, 164501.
(28) Schmidt, J.; VandeVondele, J.; Kuo, I. W.; Sebastiani, D.; Siepmann, J. I.; Hutter, J.; Mundy, C. J. *J. Phys. Chem. B* **2009**, *113*, 11959.
(29) Kühne, T. D.; Krack, M.; Parrinello, M. *J. Chem. Theory Comput.* **2009**, *5*, 235.
(30) Kuo, I. W.; Mundy, C. J.; McGrath, M. J.; Siepmann, J. I. *J. Chem. Theory Comput.* **2006**, *2*, 1274.
(31) Neese, F. *ORCA*; University of Bonn: Bonn, Germany, 2009.
(32) Perdew, J. P.; Burke, K.; Ernzerhof, M. *Phys. Rev. Lett.* **1996**, *77*, 3865.
(33) Perdew, J. P.; Burke, K.; Ernzerhof, M. *Phys. Rev. Lett.* **1997**, *78*, 1396.
(34) Becke, A. D. *Phys. Rev. A* **1988**, *38*, 3098.
(35) Lee, C.; Yang, W.; Parr, R. G. *Phys. Rev. B* **1988**, *37*, 785.
(36) Miehlich, B.; Savin, A.; Stoll, H.; Preuss, H. *Chem. Phys. Lett.* **1989**, *157*, 200.
(37) Becke, A. D. *J. Chem. Phys.* **1993**, *98*, 5648.

(38) Stephens, P. J.; Devlin, F. J.; Chabalowski, C. F.; Frisch, M. J. *J. Phys. Chem.* **1994**, *98*, 11623.
(39) Becke, A. D. *J. Chem. Phys.* **1993**, *98*, 1372.
(40) Grimme, S. *J. Chem. Phys.* **2003**, *118*, 9095.
(41) Weigend, F.; Ahlrichs, R. *Phys. Chem. Chem. Phys.* **2005**, *7*, 3297.
(42) Hess, B.; Kutzner, C.; van der Spoel, D.; Lindahl, E. *J. Chem. Theory Comput.* **2008**, *4*, 435.
(43) VandeVondele, J.; Krack, M.; Mohamed, F.; Parrinello, M.; Chassaing, T.; Hutter, J. *Comput. Phys. Commun.* **2005**, *167*, 103.
(44) The CP2K depelopers group. http://cp2k.berlioz.de/ (accessed Jul 27, 2011).
(45) Goedecker, S.; Teter, M.; Hutter, J. *Phys. Rev. B* **1996**, *54*, 1703.
(46) Swope, W. C.; Andersen, H. C.; Berens, P. H.; Wilson, K. R. *J. Chem. Phys.* **1982**, *76*, 637.
(47) Humphrey, W.; Dalke, A.; Schulten, K. *J. Mol. Graphics* **1996**, *14*, 33.
(48) Allen, M. P.; Tildesley, D. J. *Computer Simulation of Liquids*; Oxford University Press: New York, 1989; p 60.
(49) Eckart, C. *Phys. Rev.* **1935**, *47*, 552.
(50) Vaara, J.; Lounila, J.; Ruud, K.; Helgaker, T. *J. Chem. Phys.* **1998**, *109*, 8388.
(51) Cohen, A. J.; Mori-Sánchez, P.; Yang, W. *Science* **2008**, *321*, 792.
(52) Mareš, J.; Liimatainen, H.; Pennanen, T. O.; Vaara, J. Submitted for publication.
(53) Neilson, G. W.; Enderby, J. E. *J. Phys. C: Solid State* **1978**, *11*, L625.
(54) Newsome, J.; Neilson, G.; Enderby, J.; Sandström, M. *Chem. Phys. Lett.* **1981**, *82*, 399.
(55) Yazyev, O. V.; Helm, L. *J. Chem. Phys.* **2007**, *127*, 84506.
(56) Ren, P.; Ponder, J. W. *J. Phys. Chem. B* **2003**, *107*, 5933.
(57) Grimme, S. *J. Comput. Chem.* **2004**, *25*, 1463.
(58) Zimmerli, U.; Parrinello, M.; Koumoutsakos, P. *J. Chem. Phys.* **2004**, *120*, 2693.
(59) Soper, A. K. *Chem. Phys.* **2000**, *258*, 121.
(60) Hura, G.; Sorenson, J. M.; Glaeser, R. M.; Head-Gordon, T. *J. Chem. Phys.* **2000**, *113*, 9140.
(61) Paesani, F.; Zhang, W.; Case, D. A.; Cheatham, T. E.; Voth, G. A. *J. Chem. Phys.* **2006**, *125*, 184507.
(62) Paesani, F.; Voth, G. A. *J. Phys. Chem. B* **2009**, *113*, 5702.
(63) Laage, D.; Hynes, J. T. *J. Phys. Chem. B* **2008**, *112*, 14230.
(64) Mills, R. *J. Phys. Chem.* **1973**, *77*, 685.
(65) Rezus, Y. L. A.; Bakker, H. J. *J. Chem. Phys.* **2005**, *123*, 114502.
(66) Woutersen, S.; Emmerichs, U.; Bakker, H. J. *Science* **1997**, *278*, 658.
(67) Jonas, J. *J. Chem. Phys.* **1976**, *65*, 582.
(68) Tielrooij, K.; Petersen, C.; Rezus, Y.; Bakker, H. *Chem. Phys. Lett.* **2009**, *471*, 71.
(69) Laage, D. *J. Phys. Chem. B* **2009**, *113*, 2684.
(70) Bakker, H. J.; Skinner, J. L. *Chem. Rev.* **2010**, *110*, 1498.
(71) Grant, D. M.; Brown, R. A. In *Encyclopedia of NMR Spectroscopy*; Grant, D. M., Harris, R. K., Eds.; Wiley: New York, 1996; p 4003.
(72) Fernández-Serra, M. V.; Artacho, E. *J. Chem. Phys.* **2004**, *121*, 11136.
(73) Sit, P. H.; Marzari, N. *J. Chem. Phys.* **2005**, *122*, 204510.
(74) Evans, M.; Refson, K.; Swamy, K.; Lie, G.; Clementi, E. *Phys. Rev. A* **1987**, *36*, 3935.
(75) de la Peña, L. H.; Kusalik, P. G. *J. Chem. Phys.* **2004**, *121*, 5992.
(76) Impey, R. W.; Madden, P. A.; McDonald, I. R. *Mol. Phys.* **1982**, *46*, 513.
(77) Novikov, A.; Lisichkin, Y.; Fomichev, N. *J. Struct. Chem+.* **1990**, *31*, 574.
(78) Swart, M.; Solà, M.; Bickelhaupt, F. M. *J. Comput. Chem.* **2011**, *32*, 1117.
(79) Torrie, G. M.; Valleau, J. P. *Chem. Phys. Lett.* **1974**, *28*, 578.
(80) Ducommun, Y.; Earl, W. L.; Merbach, A. E. *Inorg. Chem.* **1979**, *18*, 2754.